

SUPPLEMENTARY INFORMATIONS

**Fluorescence Resonance Energy Transfer between
ZnO/MgO/Carboxymethyl- β -cyclodextrin and Nile Red in HeLa
cells - biosensing applications**

B. Sikora, ^{*a} K. Fronc, ^a I. Kamińska, ^a K. Koper, ^{b,c} M. Chwastyk, ^a P. Stępień, ^{b,c} W. Paszkowicz, ^a
T. Wojciechowski, ^a K. Sobczak, ^a D. Elbaum ^a

Author Affiliations:

[a] Institute of Physics, Polish Academy of Sciences, al Lotników 32/46, 02-668 Warsaw, Poland;

[b] Institute of Genetics and Biotechnology, Faculty of Biology, University of Warsaw ul.
Pawińskiego 5a, 02-106 Warsaw;

[c] Institute of Biochemistry and Biophysics PAN ul. Pawińskiego 5a, 02-106 Warsaw

*** Corresponding author:** E-mail: sikorab@ifpan.edu.pl

SI. Synthesis and properties of ZnO/MgO nanoparticles

ZnO/MgO nanoparticles were prepared according to Figure S1. ZnO nanoparticles were synthesized from zinc acetate and NaOH.^[1,2,3] 5 mmol (1.1 g) of $\text{Zn}(\text{CH}_3\text{COO})_2 \times 2\text{H}_2\text{O}$ (Chempur, pure p.a.) was added to 570 ml of ethanol. 15 mmol (0.6 g) of NaOH was added to 500 ml of ethanol. These mixtures were sonicated at room temperature until dissolution. The reaction was initiated by the addition of a NaOH solution to a $\text{Zn}(\text{CH}_3\text{COO})_2 \times 2\text{H}_2\text{O}$ solution at about 10 °C with vigorous stirring. The mixture was kept for 15 min at this temperature and later heated to 45 °C and held for 2 h.

0.84 mmol (0.18 g) of magnesium acetate (Chempur, pure p.a.) in 130 ml of ethanol and 2.1 mmol (0.084 g) of NaOH were added to a solution of ZnO nanoparticles (sample Mg: Zn = 0.17). The synthesis was carried out at 45 °C for 17 h. The synthesized ZnO/MgO core/shell nanoparticles were centrifuged (3000 rpm, 15 min, 20 °C) and then purified three times with ethanol/heptane (1:3 ratio) to remove CH_3COO^- and Na^+ ions. Subsequently, the nanoparticles were dried at room temperature for further measurements.

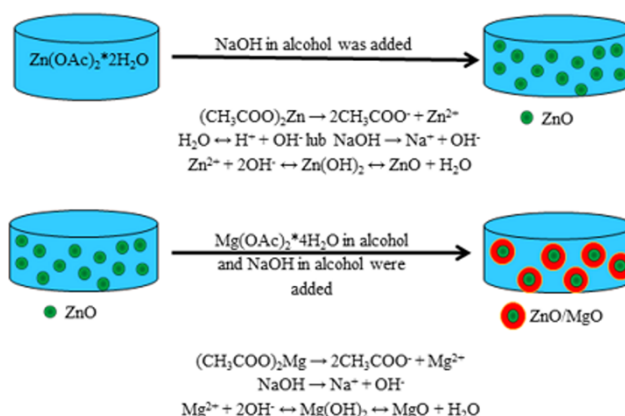


Figure S1. Synthesis of ZnO/MgO core/shell nanoparticles.

(1) Structural properties of ZnO/MgO nanoparticles

The crystalline structure and size of nanoparticles were obtained from X-ray diffraction (XRD) in a Philips X'Pert Pro Alpha1 MPD (Panalytical) diffractometer in the range of angles 2θ between 10 ° and 150 ° for 15 hours.

The X-ray diffraction pattern (XRD) of ZnO/MgO nanoparticles is shown in **Figure S2** and indicates a hexagonal wurtzite crystal structure of the nanocrystals. There was no reflection characteristic of cubic MgO derived from the plane (200) - 42.9° and from the plane (220) - 62.3°, probably due to enforced hexagonal structure in thin MgO coating by the ZnO core.

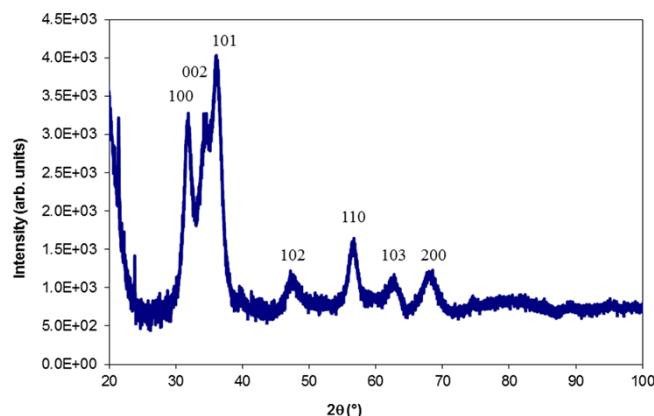


Figure S2. The X-ray diffraction spectra (wavelength 1.5 Å) of ZnO/MgO core/shell nanoparticles in powder. The ratio of Mg to Zn was 0.17.

Due to the fact that the presence of MgO layer does not affect the width at half maximum (FWHM) of the XRD reflections in the core/shell structures,^[4,5] the size of ZnO/MgO nanocrystals can be determined from the Scherrer equation:

$$t = \frac{0,9\lambda}{B \cos \theta} \quad (1)$$

where: t - particle diameter (Å);

λ - wavelength (1.54 Å);

B - width at half maximum (radians).

Size was determined from the peak 102 broadening and found to be about 5 nm.

Transmission electron microscope (TEM) JEOL JEM200EX, working at an accelerating voltage of 200 kV, was used to verify the crystal structure and size of the nanoparticles. Samples for TEM observation were prepared by dripping the particles sonicated solution in methanol on the copper grid coated with a carbon film.

Figure S3 shows the image of ZnO/MgO nanoparticles with sizes of about 6 nm (**Figure S4**) obtained from the transmission electron microscope (TEM). High-resolution image of the ZnO/MgO nanoparticles with crystalline planes that confirm hexagonal wurtzite ZnO structure is included on the right side of **Figure S3**. TEM images did not reveal the presence of MgO cubic shell (similar to the XRD measurement), probably because it was relatively thin (less than a critical value for the relaxation from the hexagonal to the cubic structure). Zinc oxide enforces hexagonal structure of magnesium oxide, as has been observed in the ZnO/MgO wires^[6] and other semiconductor nanocrystals of the II-VI core/shell type.^[7,8]

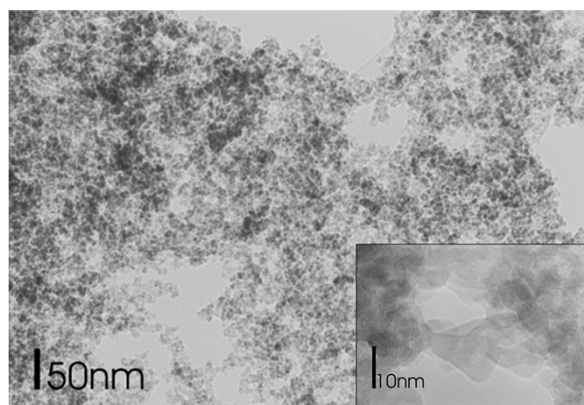


Figure S3. ZnO/MgO core/shell nanoparticles TEM image. Right: high-resolution TEM image of crystallographic planes of ZnO.

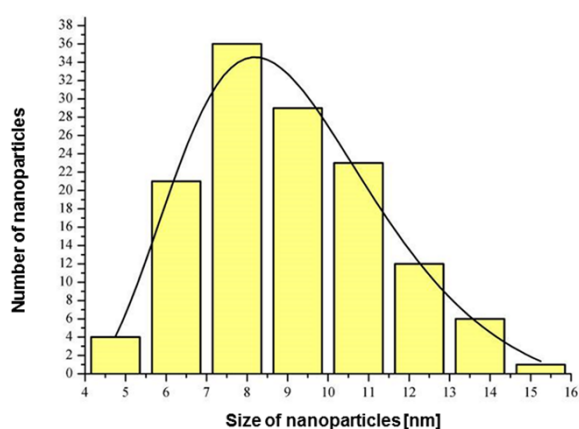


Figure S4. Histogram of nanoparticles sizes obtained from TEM measurements.

Mg:Zn atomic ratio was obtained from X-ray energy dispersive spectroscopy (EDX) spectra of ZnO/MgO nanoparticles by using (EDX)-system QUANTAX 400 Bruker coupled to a FE-SEM Carl Zeiss microscope. Mg:Zn atomic ratio was 0.13 ± 0.004 which is consistent with the atomic ratio of Mg:Zn = 0.17 used in the reaction (**Figure S5**).

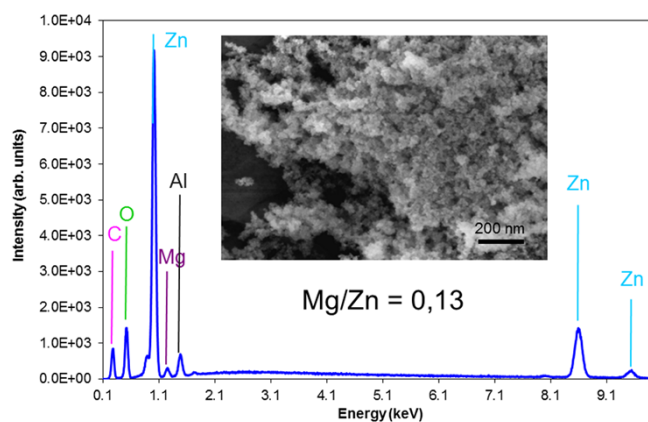


Figure S5. EDX spectrum of ZnO/MgO core/shell nanoparticles (Mg:Zn = 0.17). Inside: SEM image of ZnO/MgO powder.

(2) Absorption and emission properties of ZnO/MgO nanoparticles and their aggregation and stability

Absorption spectra were measured at room temperature as a function of storage time of ZnO/MgO nanoparticles in ethanol and water (**Figure S6A** and **Figure S7A**). The absorption spectra of ZnO/MgO solutions show that the absorption edge does not move significantly towards the higher wavelength, even after 30 days in the case of a solution in ethanol and 42 days in the case of a solution in water. This demonstrates size stability of the ZnO/MgO crystallites. In the case of MgO free ZnO nanoparticle (unshelled) solutions, a rapid increase in the nanoparticles size was observed.

The intensity of the ZnO/MgO nanoparticles luminescence (**Figure S6B** and **Figure S7B**) does not change significantly with prolonged storage time, even after 42 days. Small changes observed for the nanoparticles ethanol suspensions resulted from their sedimentation. Luminescence spectra of ZnO/MgO nanoparticles remained unchanged even after 42 days, implying that the MgO passivation effectively prevents further growth of the nanoparticles in the solution. These data are consistent with those previously published.^[2,9]

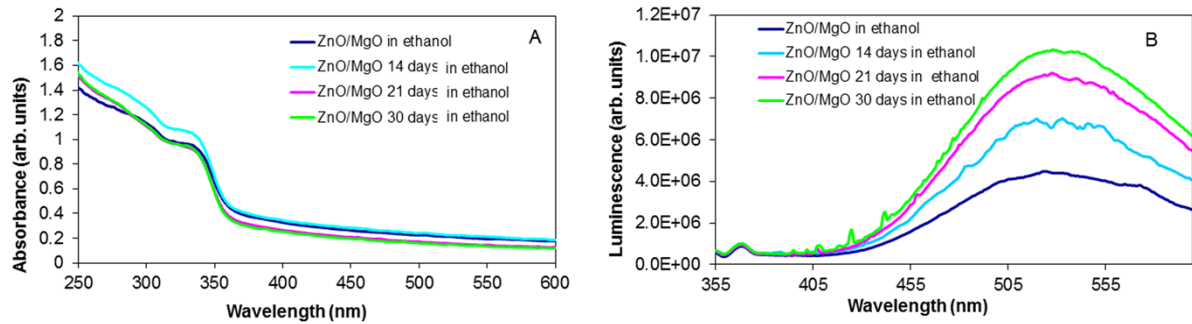


Figure S6. Plots of **A:** absorbance and **B:** luminescence of ZnO/MgO nanoparticles (Mg: Zn = 1:1) as a function of storage time. Nanoparticle concentration: 7.15 mg/ml in ethanol.

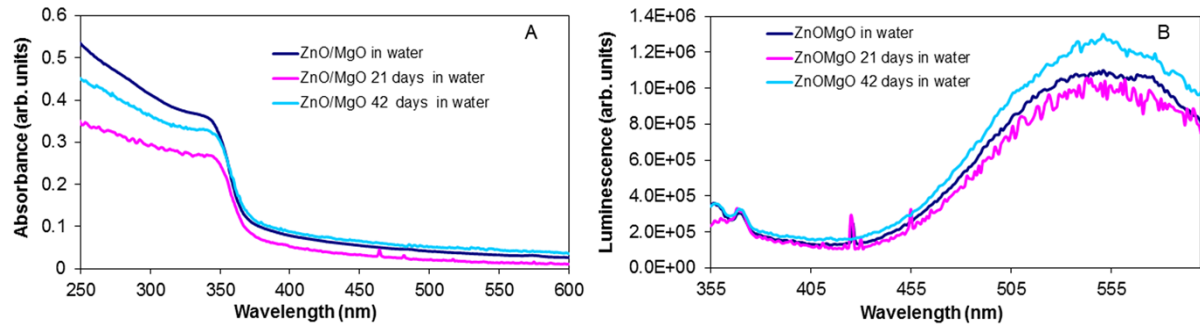


Figure S7. Plots of **A:** absorbance and **B:** luminescence of ZnO/MgO nanoparticles (Mg: Zn = 1:1) as a function of storage time. Nanoparticle concentration: 0.076 mg/ml in water.

The size of the ZnO core in ethanol and water was determined from the absorption spectra and the effective mass approximation ^[10] for various storage periods (**Table S1**).

Table S1. ZnO core size in ZnO/MgO nanoparticles (Mg:Zn = 1:1) versus time of storage in ethanol and water.

	0 days	14 days	21 days	30 days	42 days
	$2r$ [nm]	$2r$ [nm]	$2r$ [nm]	$2r$ [nm]	$2r$ [nm]
ethanol	6.2	6,2	5.9	5,9	-
water	6.1	-	6.2	-	6.4

Earlier studies reported that the MgO layer not only stabilizes the nanoparticles, but also enhances their luminescence. The green ZnO/MgO luminescence was enhanced by 30% compared to the ZnO luminescence.^[2] Formation of type I of heterojunction in the core/shell structure can be responsible for the phenomenon.^[6,11]

Excitation spectra of the ZnO/MgO solutions, detected at 555 nm and 375 nm (**Figure S8**), overlap with the excitation spectrum of the ZnO nanoparticles.

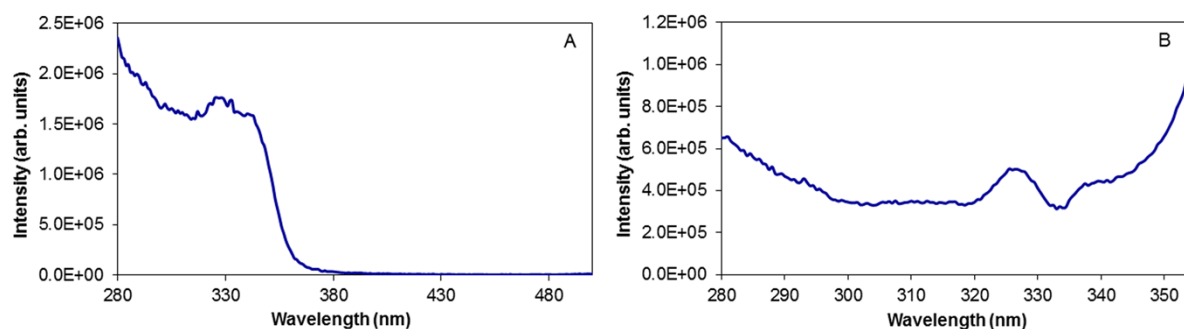


Figure S8. Excitation spectra of ZnO/MgO nanoparticles (Mg: Zn = 1:1) measured at a wavelength of **A**: 555 nm and **B**: 375 nm. Concentration of the nanoparticles was 0.2 mg/ml in ethanol.

Stability of the nanoparticles in physiologically relevant phosphate buffers were examined, for various incubation time and concentration of phosphate ions. The results are shown in **Figure S9**. Despite changes in the optical properties of ZnO/MgO nanoparticles, Rakshit S. et. al^[12] have claimed stability of the nanoparticles. Our results reviled that in solutions with low concentrations of phosphate ions (2 mM and 5 mM), the ZnO/MgO nanoparticles degraded until reached the equilibrium between the nanoparticles and the phosphate ions. At higher concentrations (10 mM, 25 mM), the nanoparticles decomposed almost completely after two hours. Hence we concluded that the ZnO/MgO nanoparticles could be used in buffers of 2 mM and 5 mM phosphate concentration (physiological concentration).

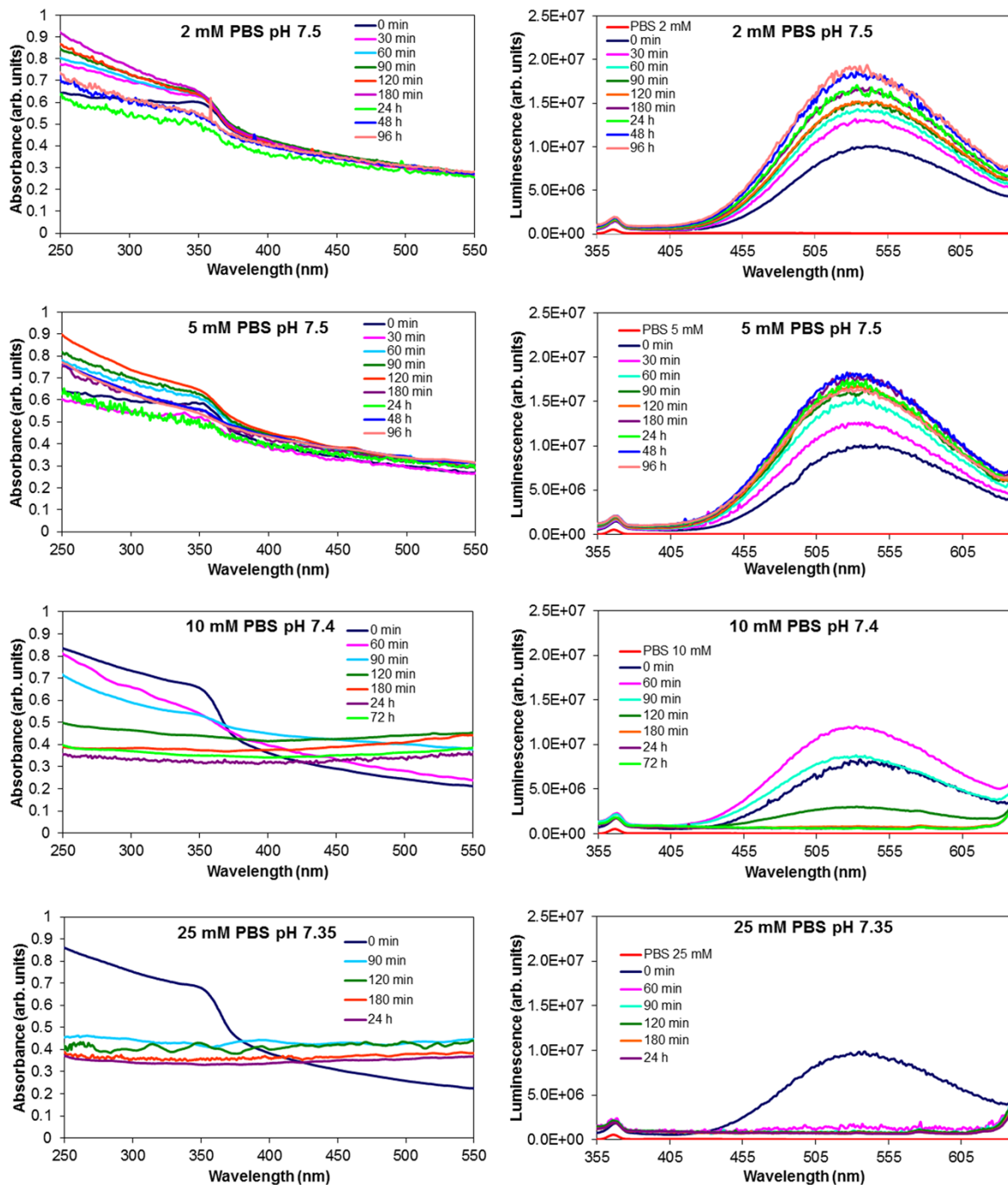


Figure S9. Absorbance (left side) and luminescence (right side) spectra of the ZnO/MgO nanoparticles at 2 mM, 5 mM, 10 mM, 25 mM phosphate buffer at pH about 7.4, depending on the time of incubation. Concentration of the nanoparticles: 0.115 mg/ml. Excitation wavelength: 325 nm.

SII. Coating of ZnO/MgO nanoparticles by carboxymethyl- β -cyclodextrin (CMCD)

ZnO/MgO core/shell nanoparticles were covered by CMCD. A threefold excess of CMCD (1.3 mmol, 2 g) dissolved in 10 ml of water was added into the ZnO/MgO solution (0.423 mmol, 0.032 g) in 40 ml of DMSO, as previously described.^[12] The reaction was carried out for 6 h at 50 °C. The solution was cooled to room temperature and treated with excess

acetonitrile (150 mL) to precipitate it into a white powder. The powder was isolated by centrifugation (3000 rpm, 15 min, 20 °C) and then cleaned with a solution of 3:1 water:DMSO, 3:1 water:acetone. The powder was dried and prepared for further analysis.

A unique feature of the ZnO/MgO nanoparticles coated with CMCD lies in retaining the ability of the cyclodextrin cavities to include small hydrophobic molecules, after they are anchored to the nanoparticles surface. Cyclodextrin did not change the optical properties of ZnO/MgO nanoparticles (**Figure S10**).

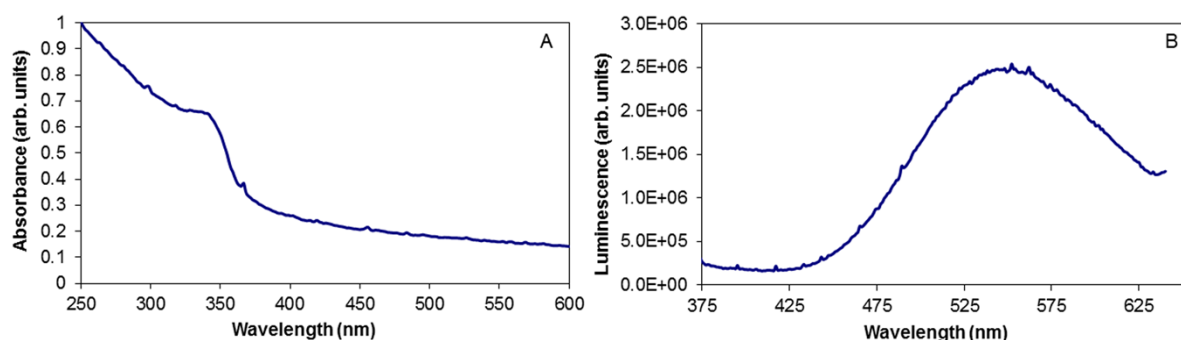


Figure S10. **A:** Absorbance spectrum and **B:** luminescence spectrum of ZnO/MgO core/shell nanoparticles coated with carboxymethyl- β -cyclodextrin. The concentration of the nanoparticles was 20 mg/ml in water. Wavelength excitation was 356 nm.

SIH. FRET between ZnO/MgO nanoparticles and Nile Red

(1) Fluorescence Resonance Energy Transfer between ZnO/MgO core/shell nanoparticles and Nile Red

Comparative examination of the ZnO/MgO/CMCD/Nile Red complex FRET properties was performed applying two excitation laser sources: at 355 nm and 705 nm using a confocal microscope (**Figure S11**).

As judged from **Figure 11**, the change of the excitation wavelength from 355 nm to 705 nm does not alter the luminescence originating from the ZnO defects (about 545 nm). Departure from the UV excitation has practical biological advantage as it may reduce tissue damage and cellular autofluorescence.

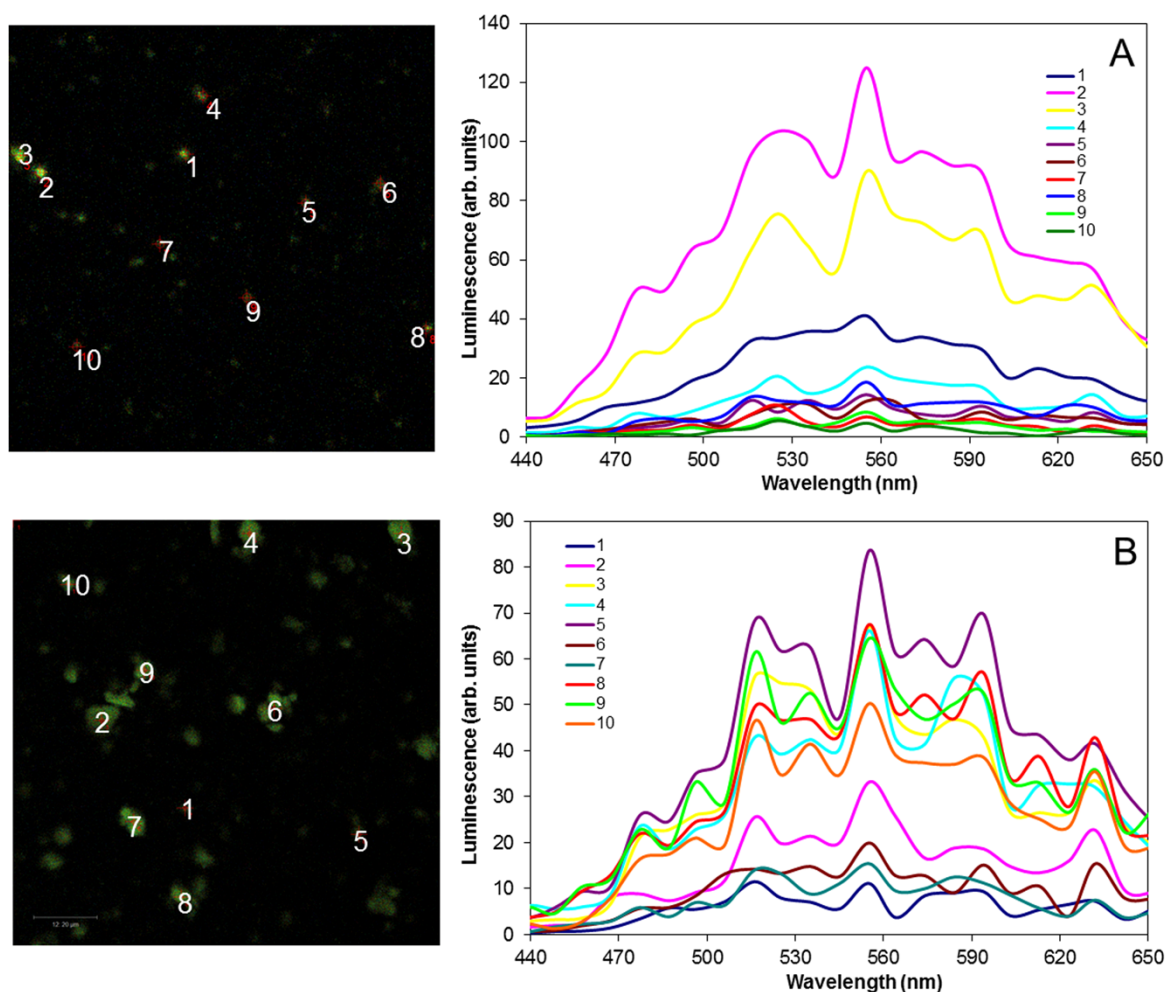


Figure S11. A: The luminescence of ZnO/MgO/CMCD nanoparticles (20 mg/ml in water) with excitation wavelength of 355 nm, laser power: 0.3 mW; B: the luminescence of ZnO/MgO/CMCD nanoparticles (20 mg/ml in water) with excitation wavelength of 705 nm, laser power: 201,6 mW (maximum pulse width: 140 fs, the pulse frequency: 80 MHz).

(2)FRET between ZnO/MgO nanoparticles and Nile Red, measurements of the luminescence decay time

The luminescence decay time of the visible light from ZnO/MgO/CMCD (donor) and the donor in the presence of Nile Red resulting from 705 nm multiphoton excitation was measured, to complement the stationary fluorescence measurements. A 580/70 nm filter matched to the green luminescence of ZnO defects was applied. Decay profiles were recorded in the presence of various concentrations of the acceptor (**Figure S12**). Two exponential decay curve were fitted, using the PICOQIANT program, to the recorded luminescence decay times curves (**Figure S13**). Luminescence decays times with their amplitudes were obtained from the alignment. Then the average values of the luminescence decay times were estimated by using the equation (2)^[13] (**Table S2 and Figure S14**).

$$\langle \tau \rangle = \frac{\sum_i \alpha_i \tau_i}{\sum_i \alpha_i} \quad (2)$$

where: α - decay time amplitude;

τ_i - luminescence decay time.

Table S2 and **Figure S14** summarize the average donor luminescence decay time decrease with increasing concentration of Nile Red, as expected from the energy transfer.

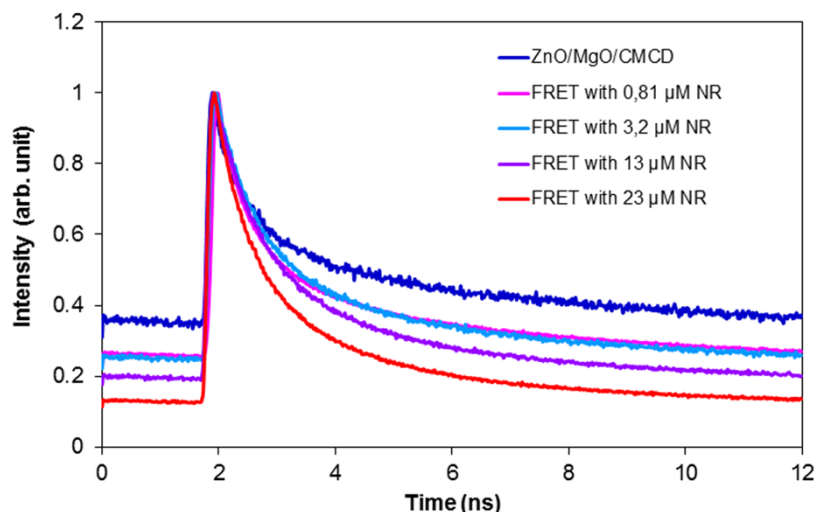


Figure S12. Luminescence decay curves of ZnO/MgO/CMCD depending on the Nile Red concentration. The concentration of ZnO/MgO/CMCD nanoparticles was 20 mg/ml in water, and the concentration of Nile Red was 0.81 μ M, 3.2 μ M, 13 μ M, 23 μ M. Excitation wavelength was 705 nm (4.0-8.1 mW laser power, maximum pulse width: 140 fs, the pulse frequency: 80 MHz). Filter 580/70 nm. The results were normalized to 1.

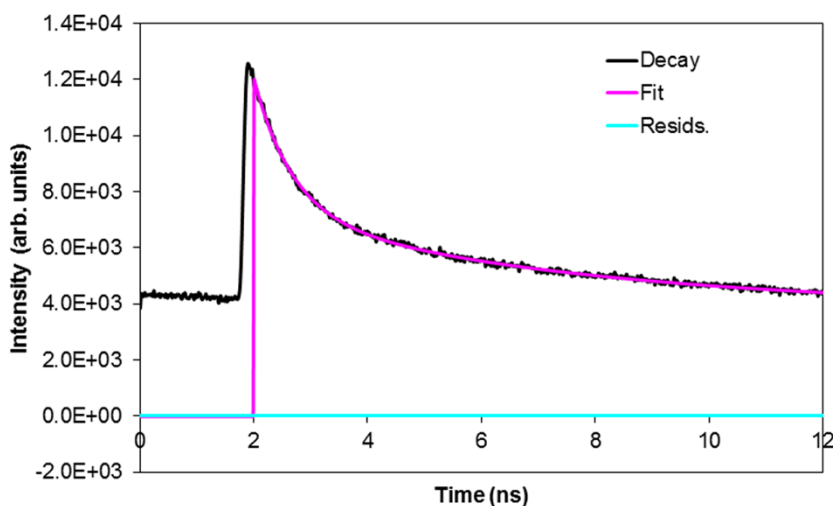


Figure S13. Example of two-exponential fit to the decay curve of the ZnO/MgO/CMCD nanoparticles (20 mg/ml) luminescence in water. Excitation wavelength was 705 nm (4.0-8.1 mW laser power, maximum pulse width: 140 fs, the pulse frequency: 80 MHz). Filter 580/70 nm.

Table S2. Luminescence decay times and the mean luminescence decay times of ZnO/MgO/CMCD nanoparticles in the presence of varying Nile Red amounts in water. Values was determined from a two-exponential function fit to the curves in Figure S12. Excitation wavelength was 705 nm (4.0-8.1 mW laser power). Filter 580/70 nm. (The confidence level was P = 0.9545).

	t_1 [ns]	t_2 [ns]	$\langle t \rangle$ [ns]
ZnO/MgO/CMCD	4.78 ± 0.56	$0.56 \pm 0,05$	2.34 ± 0.37
FRET with 0,81 μM Nile Red	4.31 ± 0.06	$0.61 \pm 0,02$	2.18 ± 0.12
FRET with 3,2 μM Nile Red	3.98 ± 0.43	$0.72 \pm 0,10$	2.09 ± 0.28
FRET with 13 μM Nile Red	3.49 ± 0.24	$0.74 \pm 0,08$	1.85 ± 0.12
FRET with 23 μM Nile Red	3.14 ± 0.51	$0.71 \pm 0,05$	1.64 ± 0.22

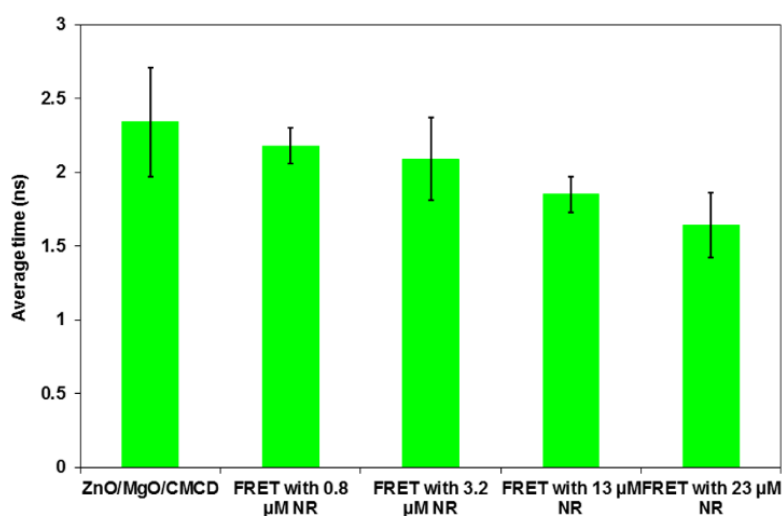


Figure S14. Average luminescence decay times of ZnO/MgO/CMCD nanoparticles in the presence of varying amounts of Nile Red in water determined from a two-exponential function fit to the curves in Figure S12. Excitation wavelength was 705 nm (4.0-8.1 mW laser power). Filter 580/70 nm.

SIIV. FRET Efficiency

(1) *FRET efficiency - stationary measurements*

FRET was calculated from the formula:

$$Q = \frac{I_{ZnO} - I_{ZnO-NR}}{I_{ZnO}} \quad (3)$$

where: I_{ZnO} - intensity of luminescence of the donor ZnO/MgO/CMCD molecule in water in the absence of Nile Red;

I_{ZnO-NR} - intensity of luminescence of the donor ZnO/MgO/CMCD molecule in water in the present of Nile Red.

Resonance Energy Transfer efficiency was calculated from the formula:

$$Q = \frac{k_{ZnO-NR}}{k_{ZnO-NR} + \tau_{ZnO}^{-1}} = \frac{R_0^6}{R_0^6 + r^6} \quad (4)$$

where: τ_{ZnO} - the decay time of the ZnO/MgO (donor) luminescence in the absence of Nile Red (acceptor);

k_{ZnO-NR} - the rate constant of the ZnO/MgO/CMCD (donor) emission in the presence of Nile Red (acceptor);

r - the distance between the donor and acceptor;

R_0 - the critical distance (Forster radius) at which transfer and spontaneous decay of the excited donor are equally probable, $k_{ZnO-NR} = \tau_{ZnO}^{-1}$.

R_0 can be determined experimentally from the spectroscopic data:

$$R_0 = \frac{9000(\ln 10)\kappa^2\gamma_D^0}{128\pi^5 N_A \eta^4} J(\lambda) \quad (5)$$

where: κ^2 - indicative factor, which is 2/3 for randomly oriented donor and acceptor dipoles;

γ_D^0 - quantum yield of the donor in the absence of acceptor;

N_A - Avogadro's number;

η - refractive index;

$J(\lambda)$ - integral of the overlap of the donor emission with acceptor absorption.

Spectral overlap of the donor and acceptor emission is given by:

$$J(\lambda) = \int_0^\infty I_D(\lambda)\varepsilon_A(\lambda)\lambda^4 d\lambda \quad (6)$$

where: $I_D(\lambda)$ - normalized luminescence spectrum of the donor (ZnO/MgO/CMCD);

$\varepsilon_A(\lambda)$ - absorption coefficient of the acceptor (Nile Red).

Spectroscopically determined value of R_0 is 3.4 nm for ZnO/MgO/CMCD/Nile Red.^[12] For the donor interacting with several acceptors, if the energy transfer to each acceptor can be considered as an independent event, the transfer efficiency can be expressed by the equation:^[14]

$$Q = \frac{nR_0^6}{nR_0^6 + r^6} \quad (7)$$

where: n - number of acceptor molecules.

The value of r , the distance between donor and acceptor in ZnO/MgO/CMCD/Nile Red system, may be determined by fitting the equation (7) to the experimentally observed relationship between the FRET efficiency and the acceptor concentration (solid line on the graph, **Figure S15**). Determined by this method the value of r was 3.4 nm. This value differed from the value determined earlier by Rakshit and colleagues,^[12] which was $r = 4.3$ nm. The nanoparticle size, MgO shell thickness and CMCD layer thickness could be responsible for the observed differences.

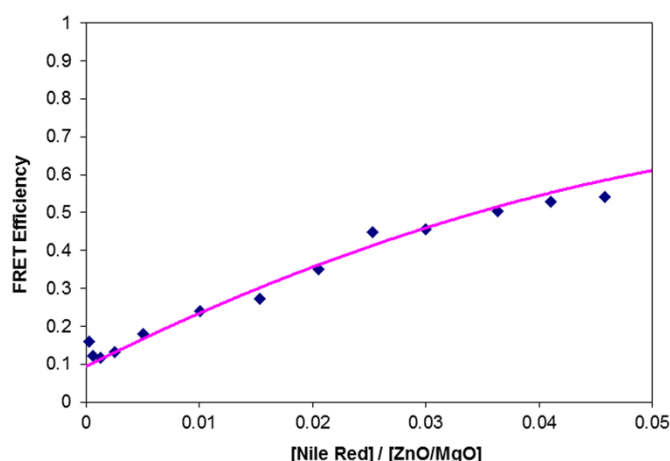


Figure S15. FRET efficiency changes depending on the concentration of acceptor (Nile Red). The donor concentration is constant. Dark points: the experimental data. Solid line: the best fit of equation (7) to the experimental data.

The FRET in the ZnO/MgO/CMCD/Nile Red complex originates from the ZnO defects emission, wherein the spectral position is not dependent on particle size. Fluctuations in the size of the nanoparticles did not affect on the FRET efficiency as opposed to the situation when we use quantum dots in which the spectral position of the emission is very sensitive to the size of the quantum dots.

Another unique feature of the FRET between the ZnO/MgO/CMCD and Nile Red is the fact that the donor and acceptor are held together by supramolecular interactions. Nile Red

acceptor molecules create inclusion complexes with the cavities of cyclodextrin covering ZnO/MgO nanoparticles. Interactions between Nile Red and cavities of cyclodextrins are of dispersive in their nature.

(2) FRET efficiency - decay time measured

FRET efficiency Q may be calculated by the formula (8), provided that two-exponential decay is used and, instead of decay times the mean decay times are used (9):

$$Q = 1 - \frac{\tau_D}{\tau_D^0} = 1 - \frac{\phi_D}{\phi_D^0} \quad (8)$$

where: Q - FRET efficiency;

τ_D - the donor fluorescence decay time in the presence of acceptor;

τ_D^0 - the donor fluorescence decay time in the absence of acceptor;

ϕ_D - quantum yield of the donor in the presence of acceptor;

ϕ_D^0 - quantum yield of the donor in the absence of acceptor.

$$Q = 1 - \frac{\langle \tau_{D-A} \rangle}{\langle \tau_D \rangle} \quad (9)$$

where: $\langle \tau_{D-A} \rangle$ and $\langle \tau_D \rangle$ - the average lifetimes of the ZnO/MgO (donor) in the presence and absence of Nile Red.

FRET efficiencies from the luminescence decay time was determined and compared with the FRET efficiencies determined from the stationary luminescence spectra (**Figure S16**).

The FRET efficiency determined from the stationary luminescence spectra of nanoparticles is higher than the efficiency determined from the luminescence decay time. The efficiency in both cases have comparable values for low Nile Red concentrations. The efficiency at excitation of 705 nm is about 15% lower than for 356 nm excitation for larger Nile Red concentrations.

The distance (r) value of the donor from the acceptor in ZnO/MgO/CMCD/Nile Red system may be determined by fitting the equation (7) to the experimentally observed relationship between the FRET efficiency and the acceptor concentration (**Figure S17**), as was determined for the FRET efficiency from stationary luminescence spectra (**Figure S15**). The value of r determined by this method was 3.4 nm. The r value is exactly the same as the value determined from the stationary luminescence spectra.

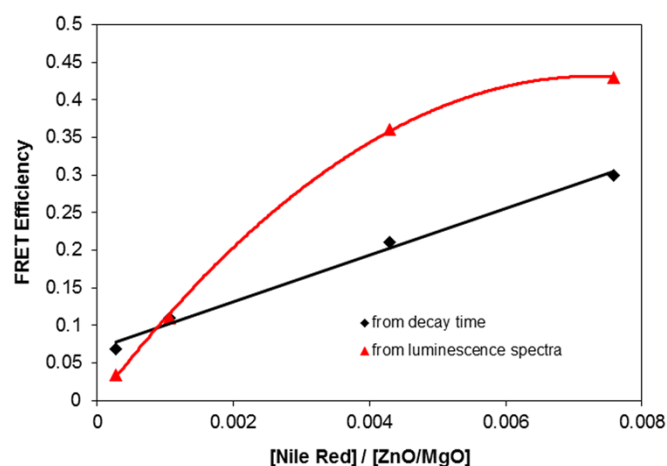


Figure S16. The FRET efficiency calculated from the average luminescence decay times of ZnO/MgO/CMCD nanoparticles in the presence of varying amounts of Nile Red in water and the FRET efficiency calculated from the stationary luminescence spectra of the nanoparticles in the presence of varying amounts of Nile Red.

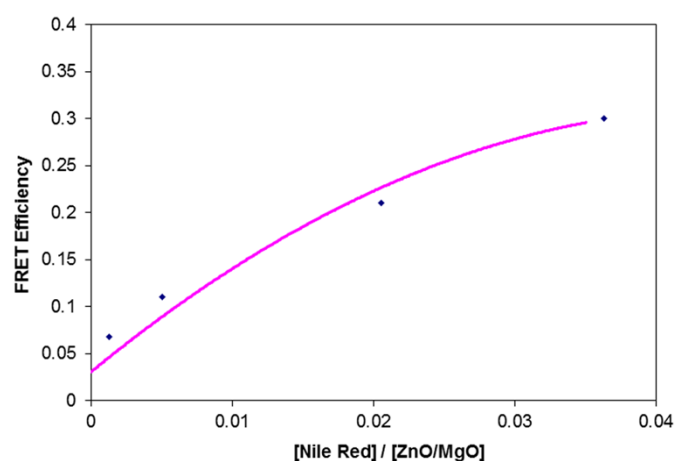


Figure S17. Changes in FRET efficiency depending on the concentration of acceptor (Nile Red). The donor concentration is constant. Dark points: the experimental data. Solid line: the best fit equation (5) to the experimental data.

The FRET between ZnO/MgO/CMCD nanoparticles and Nile Red has some unique properties, which distinguishes it from similar processes using quantum dots:

1). In contrast to quantum dots, the energy transfer in ZnO/MgO/CMCD/Nile Red complex does not come from the excitons emission but from the defect emission of ZnO. Emission in the visible range of ZnO/MgO nanocrystals is not directly related to the spectrum of "absorption", because it comes from the recombination of carriers which are generated by excitation of the energy gap and then trapped in the trap states that lie just below the conduction band or above the valence band.^[1] For this reason, the visible emission spectrum of the nanoparticles does not depend on their size, as in the case of quantum dots, and therefore their size will not directly affect the FRET efficiency.

2). Another unique feature of the ZnO MgO/CMCD Nile Red complex is the lack of a direct bond between the donor (ZnO/MgO/CMCD) and the acceptor. The donor with the acceptor are held together by supramolecular interactions. Nile Red acceptor molecules form inclusion complexes with the cavities of cyclodextrin covering ZnO/MgO nanoparticles.

SIV. Fluorescence Energy Transfer inside the HeLa cells

(1) Introducing of ZnO/MgO/CMCD/Nile Red into the HeLa cells

The transfection protocol was developed based on information provided by the manufacturer.

Step 1. Preparation of 10 ml of an aqueous solution containing 0.2 g of ZnO/MgO/CMCD nanoparticles (concentration 20 mg/ml) and 0.33 ml of 0.6 mM Nile Red solution (concentration 16 μ M). For controls, ZnO/MgO nanoparticles solution was used at the concentration of 10 mg/ml and a Nile Red solution at the concentration of 16 μ M.

Step 2. 10 μ l of a given concentration of the nanoparticles was dissolved in 500 μ l miliR H₂O.

Step 3. 20 μ l of Lipofectamine 2000 was dissolved in 500 μ l miliR H₂O.

Step 4. The Lipofectamine solution was left to incubate for 15 minutes.

Step 5. Both solutions were mixed together and left to incubate for additional 20 minutes.

Step 6. 250 μ l of the solution was added to each to 10 cm² dish.

Step 7. The cells were placed back in the incubator for 2 h.

Step 8. Finally, the medium was switched to fresh DMEM.

Microscopic samples were fixed according to the following protocol:

Step 1. Buffers:

- PBS-A (0.2 g KCl, 0.2 g KH₂PO₄, 8.0 g NaCl, 2.2 g Na₂HPO₄·7 H₂O in 1 l H₂O);
- PBS-G (0.75 g glycine in 100 ml PBS-A);
- Fix Buffer (3.70 g paraformaldehyde in 100 ml PBS-A) - stirred and heated to 50 °C, filtered through a 0.22 μ m filter.

Step 2. Procedure:

- All buffers were preheated to 37 °C before use;
- Throughout the fixation process the samples were kept at 37 °C;
- At no point in the procedure the samples can be allowed to dry out;
- Aspirate the medium and fix samples with Buffer for 15 min at 37 °C;
- Rinse once with PBS-G for 5 min at 37 °C;
- Rinse twice with PBS-A for 5 min at 37 °C.

(2) Negative Controls: ZnO/MgO/CMCD (no acceptor) and Nile Red (no donor) inside the cells

The results of the control (donor only) measurements internalized in HeLa cells were shown. **Figure S18** depicts ZnO/MgO/CMCD nanoparticles inside the cells. **Figure S19** illustrates the internalized acceptor. Excitation wavelength was 355 nm. **Figure S20** reports autofluorescence of HeLa cells.

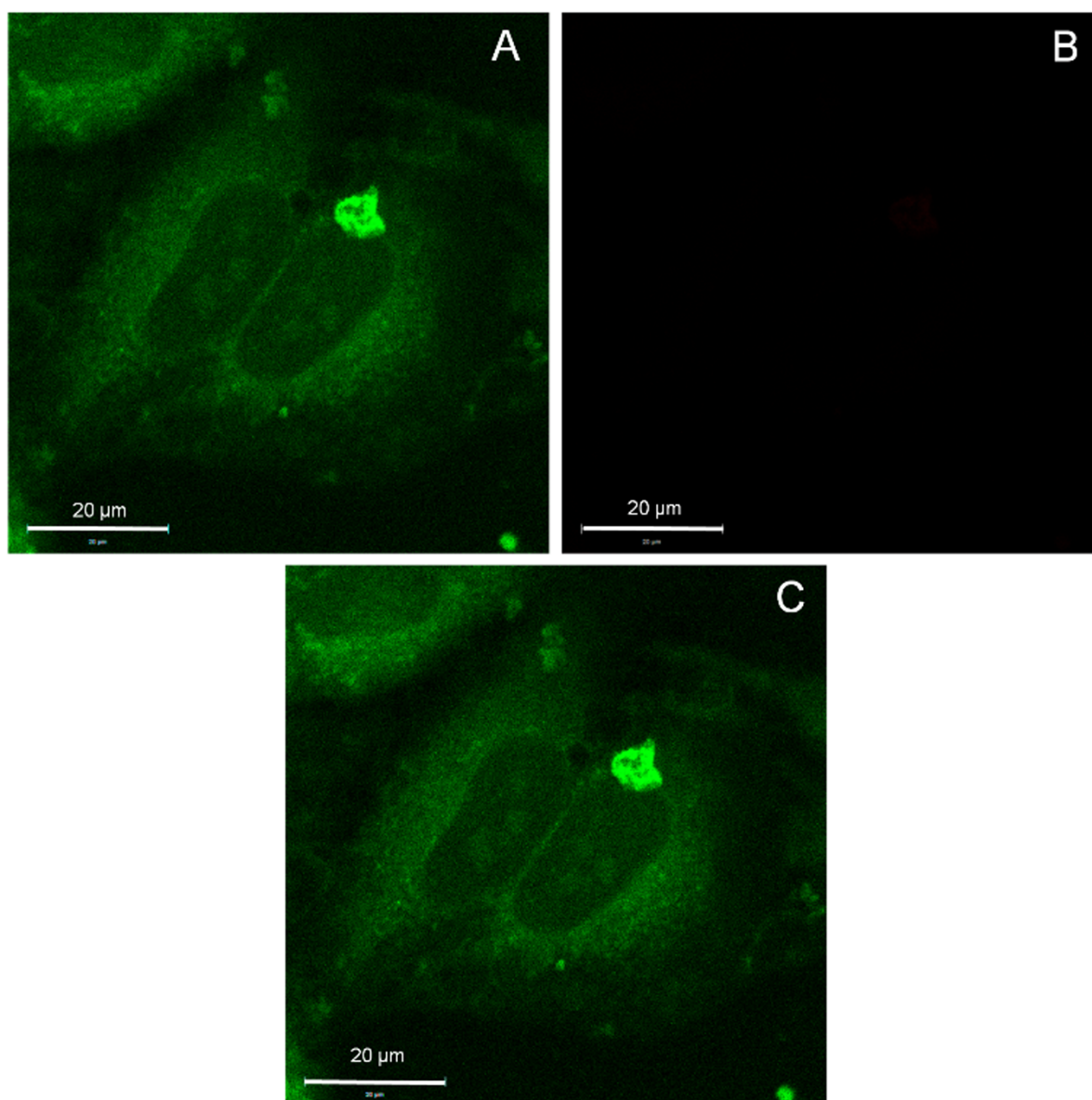


Figure S18. ZnO/MgO/CMCD nanoparticles inside HeLa cells. **A:** HeLa cells autofluorescence channel (excitation wavelength: 488 nm - CW laser, emission: 520-560 nm, 1.5 mW laser power); **B:** Nile Red luminescence channel (excitation wavelength: 355 nm - CW laser, emission: 560-700 nm, 0.3 mW laser power); **C:** imposition of the A and B channels.

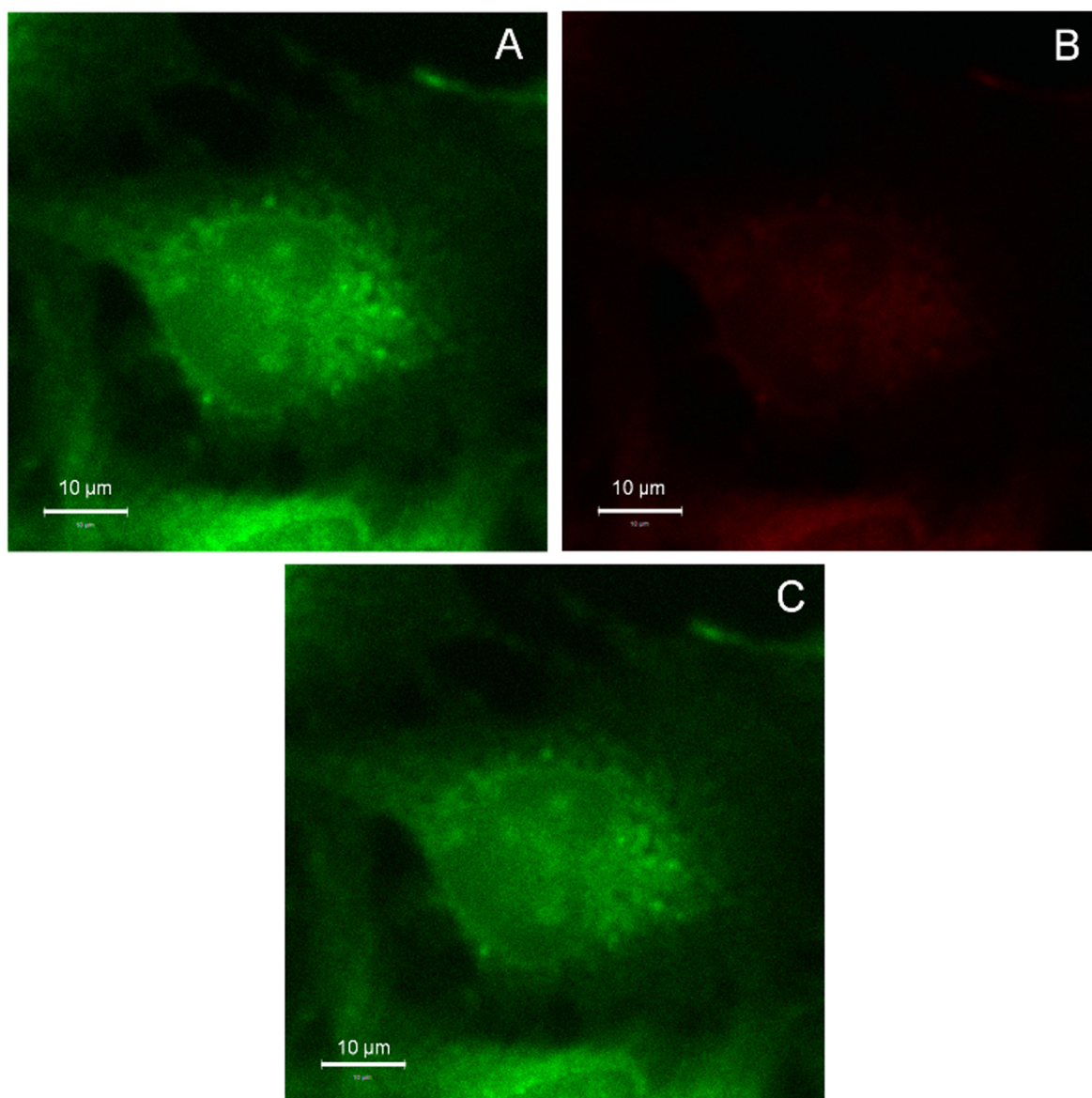


Figure S19. Nile Red inside HeLa cells. **A:** HeLa cell autofluorescence channel (excitation wavelength: 488 nm - CW laser, emission: 520-560 nm, 1.5 mW laser power); **B:** Nile Red luminescence channel (excitation wavelength: 355 nm - CW laser, emission: 560-700 nm, 0.3 mW laser power), **C:** imposition of the A and B channels.

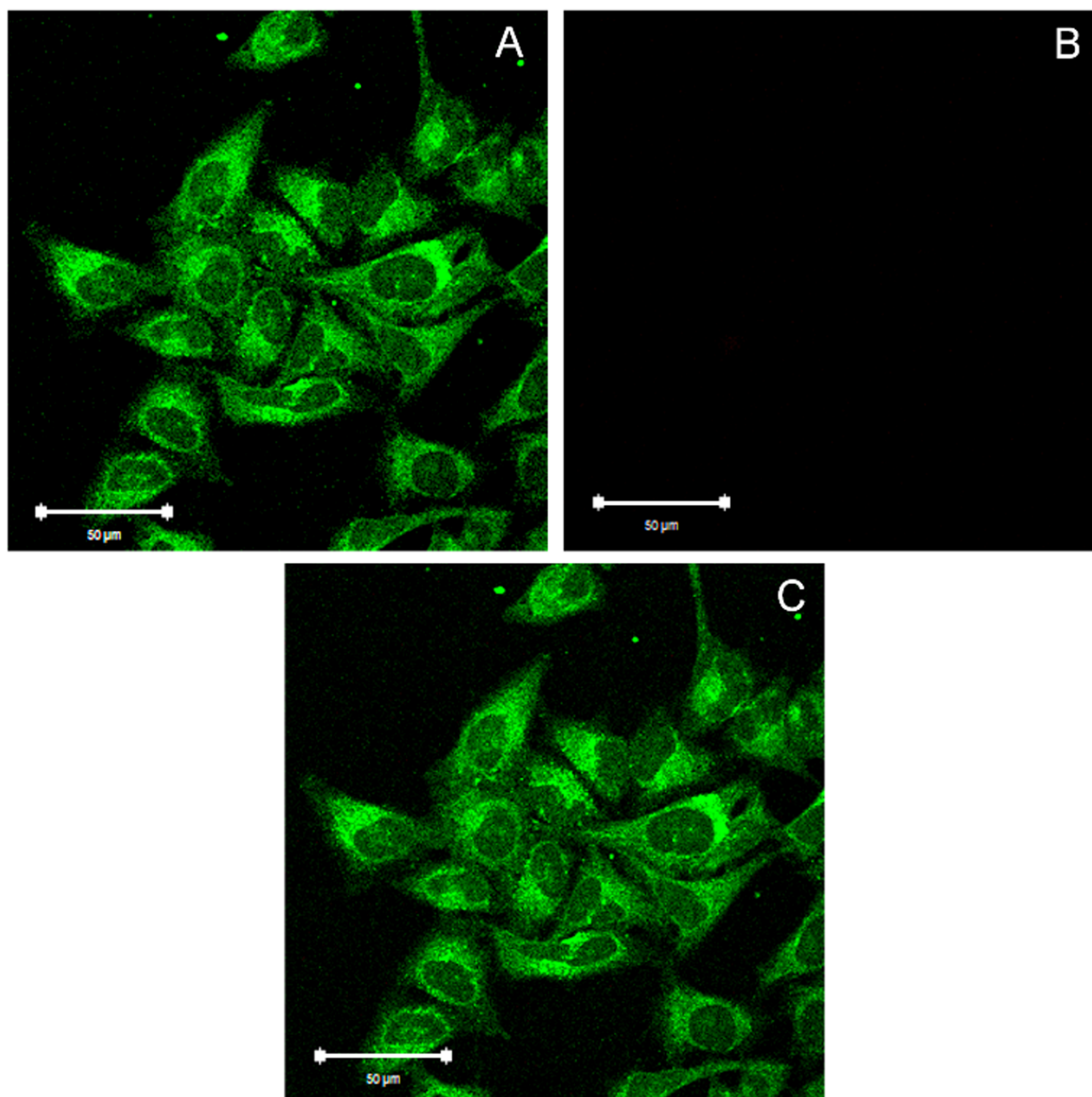


Figure S20. HeLa cells. **A:** HeLa cells autofluorescence channel (excitation wavelength: 488 nm - CW laser, emission: 511-583 nm, 0.6 mW laser power); **B:** Nile Red luminescence channel (excitation wavelength: 705 nm - laser femtosecond, emission: 601-693 nm, 8.1 mW laser power, (maximum pulse width: 140 fs, the pulse frequency: 80 MHz); **C:** the imposition of the A and B channels.

(3) Fluorescence Resonance Energy Transfer inside HeLa cells – 705 excitation wavelength

The experiments were repeated using a femtosecond multiphoton excitation at 705 nm. **Figure S21** reports the ZnO/MgO/CMCD nanoparticles inside the cells, **Figure S22** the acceptor dye inside HeLa cells. Excitation wavelength was 705 nm.

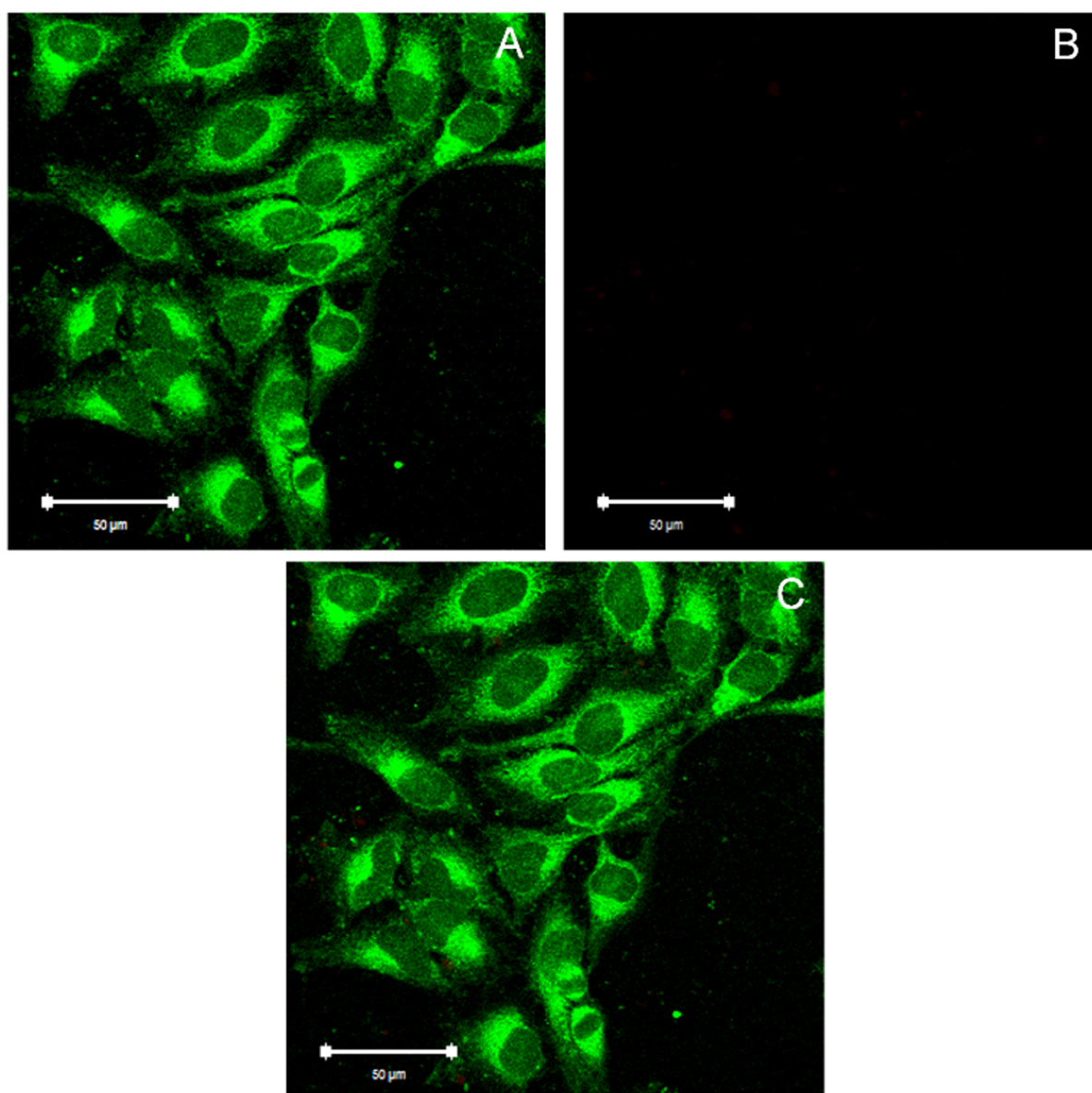


Figure S21. ZnO/MgO/CMCD nanoparticles in HeLa cells. **A:** HeLa cell autofluorescence channel (excitation wavelength: 488 nm - a CW laser, emission: 511-583 nm, 3 mW laser power); **B:** Nile Red luminescence channel (excitation wavelength: 705 nm - a femtosecond laser, emission: 601-693 nm, 8.1 mW laser power, (maximum pulse width: 140 fs, the pulse frequency: 80 MHz); **C:** the imposition of the A and B channels.

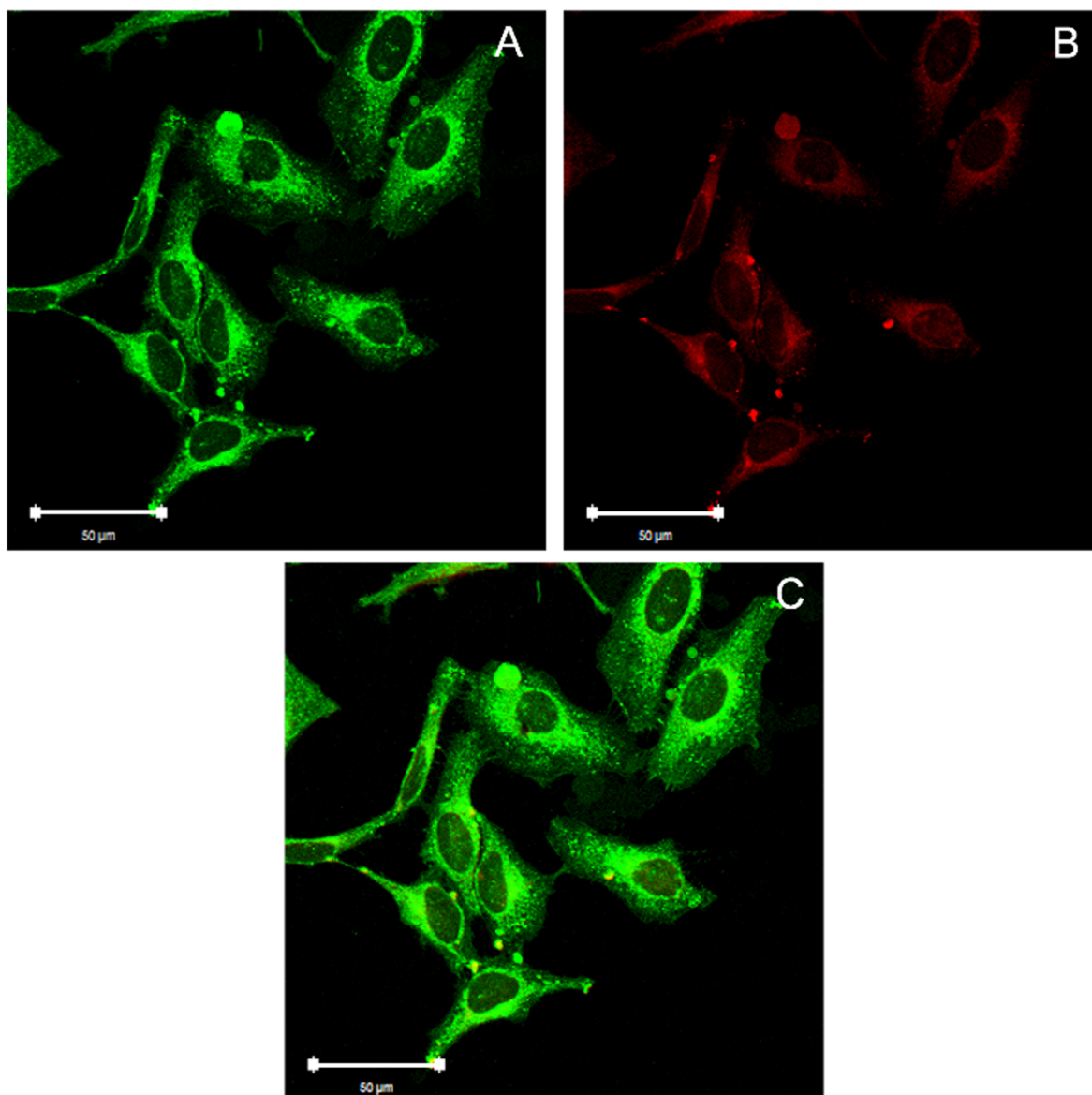


Figure S22. Nile Red in HeLa cells. **A:** HeLa cell autofluorescence channel (excitation wavelength: 488 nm - CW laser, emission: 511-583 nm, 0.18 mW laser power); **B:** Nile Red luminescence channel (excitation wavelength: 705 nm - femtosecond laser, emission: 601-693 nm, 8.1 mW laser power, (maximum pulse width: 140 fs, the pulse frequency: 80 Mz)); **C:** the imposition of the A and B channels.

(4) Spectral displacement of the Nile Red luminescence localized either outside or inside the cells

Table S3 depict changes of the Nile Red luminescence depending on the complex location (inside/outside the cell). The difference between the Nile Red luminescence (from the FRET probes) inside cells and outside cells is statistically significant (correlation coefficients > 0.9).

Table S3 The wavelength of maximum luminescence intensity of Nile Red for two locations of the fluorophore (inside/outside) the cells. Excitation wavelengths were 355 nm or 705 nm.

	inside (355 nm)	outside (355 nm)	inside (705 nm)	outside (705 nm)
Nile Red (acceptor) 3.2 μM	624 \pm 2	-	635 \pm 4	634 \pm 10
Nile Red (FRET) 3.2 μM	625 \pm 1	610 \pm 10	633 \pm 3	626 \pm 3
Nile Red (acceptor) 16 μM	623 \pm 2	605 \pm 6	632 \pm 8	629 \pm 10
Nile Red (FRET) 16 μM	625 \pm 2	603 \pm 3	634 \pm 4	617 \pm 9
Acceptor 16 μ M: inside n = 36, outside n = 5 (excitation: 355 nm); inside n = 7 outside n = 2 (excitation: 705 nm) FRET 16 μ M: inside n = 15, outside n = 26 (excitation: 355 nm); inside n = 25, outside n = 7 (excitation: 705 nm) Acceptor 3,2 μ M: inside n = 21 (excitation: 355 nm); inside n = 6, outside n=2 (excitation: 705 nm) FRET 3,2 μ M: inside n = 18, outside n = 5 (excitation: 355 nm); inside n = 14, outside n = 9 (excitation: 705 nm)				

(5) The statistical analysis of the experimental results

The statistical analysis used in this study is based on fitting the appropriate function to our experimental results. We have realized that to achieve the maximum value of the intensity in the FRET experiment, we can fit a Gaussian function to the subset of our data. The fitting was done using the method of the last squares (**Figure S23**). The results were averaged and the maximum error was evaluated using Fisher's method. The error of the intensity ratio was evaluated by the total differential method.

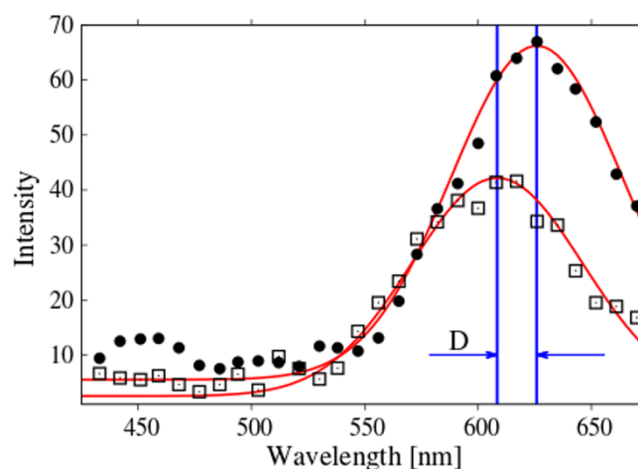


Figure S23. FRET ZnO/MgO/CMCD/Nile Red complex spectrum, depending on the position of the inside (circles) and outside of HeLa cells (squares). D is the difference between the maximum luminescence wavelengths.

(6) Evidence of Fluorescence Resonance Energy Transfer inside HeLa cells

Table S4 and **Figure S24** show the ratio of the Nile Red luminescence intensity to the intensity of luminescence at 450 nm wavelength (autofluorescence of cells) depending on the location of the fluorophore. These results were compared with the results obtained for the ZnO/MgO/CMCD (donor) inside HeLa cells, and Nile Red (acceptor) inside HeLa cells. Nile Red luminescence to autofluorescence ratios are much higher in the case of FRET complexes inside and outside of the cells compared with the acceptor when the excitation wavelength was 355 nm. These results are statistically significant (the maximum value of the error was evaluated). The standard error was calculated by the Fisher's method. In the case where higher concentration of the acceptor was used (16 mM), these ratios were higher than in the case where a smaller concentration of the acceptor was applied (3.2 mM). In the case of 705 nm excitation, there were no changes in the ratio of the Nile Red luminescence intensity to the autofluorescence. This is probably due to lower efficiency of multi-photon excitation compare to the high energy single photon donor excitation. Consequently, the FRET process is much less efficient and cannot be distinguished from the background luminescence.

Table S4 The ratio of the Nile Red maximum luminescence intensity to cells autofluorescence at an excitation wavelength of 450 nm for the fluorophore present inside or outside of the cell.

	inside (355 nm)	outside (355 nm)	inside (705 nm)	outside (705 nm)
ZnO/MgO/CMCD	0.17 ± 0.08	0.22 ± 0.08	-	-
(donor)		(background)		
Nile Red	0.30 ± 0.12	-	82.38 ± 69.12	117.54 ± 8.47
(acceptor) 3.2 μM				
Nile Red (FRET)	2.83 ± 1.23	6.48 ± 7.05	46.82 ± 44.18	60.82 ± 54.67
3.2 μM				
Nile Red	1.42 ± 0.50	1.31 ± 0.68	52.70 ± 51.40	63.53 ± 32.72
(acceptor) 16 μM				
Nile Red (FRET)	5.45 ± 2.88	17.45 ± 10.14	31.16 ± 30.51	19.43 ± 17.48
16 μM				

HeLa cells: inside n = 8, background n = 2 (excitation: 355 nm); inside n = 13, background n = 3 (excitation: 705 nm)

Donor: inside n = 25, background n = 10 (excitation: 355 nm); inside n = 17, background n = 11 (excitation: 705 nm)

Acceptor 16 μM: inside n = 36, outside n = 5 (excitation: 355 nm); inside n = 7, outside n = 2 (excitation: 705 nm)

FRET 16 μM: inside n = 15, outside n = 26 (excitation: 355 nm); inside n = 25, outside n = 7 (excitation: 705 nm)

Acceptor 3,2 μM: inside n = 21 (excitation: 355 nm); inside n = 6, outside n=2 (excitation: 705 nm)

FRET 3,2 μM: inside n = 18, outside n = 5 (excitation: 355 nm); inside n = 14, outside n = 9 excitation: 705 nm)

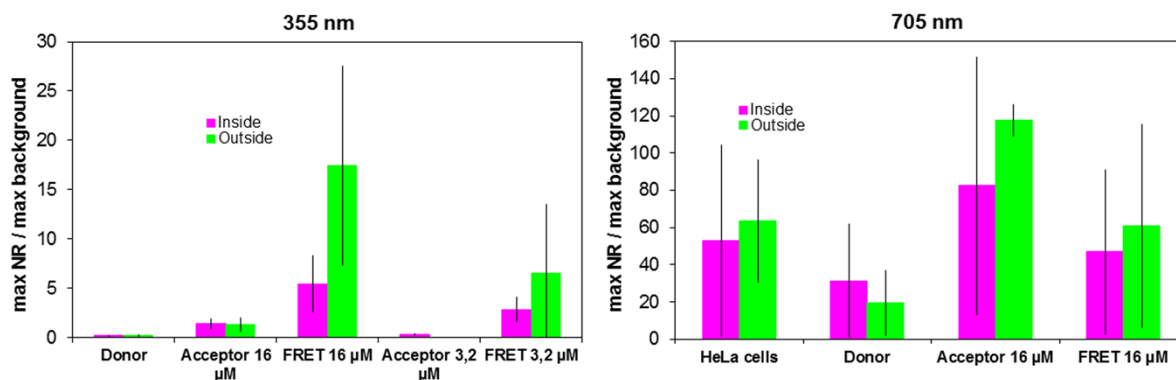


Figure S24. The ratio of the Nile Red luminescence intensity to the cell autofluorescence intensity at a 450 nm of excitation, depending on the position of the fluorophore inside/outside HeLa cells. Nanoparticles concentration was 20 mg/ml, Nile Red concentration was 16 μ M or 3.2 μ M.

Bibliography

- 1 B. Sikora, K. Fronc, I. Kamińska, K. Koper, P. Stępień, D. Elbaum *J. Phys.: Condens. Matter*, 2013, **25**, 194104-1;
- 2 J.-J. Lee, J. Bang, H. Yang, *J. Phys. D: Appl. Phys.* 2009, **42**, 025305-1;
- 3 D. Bera, L. Qia, P. H. Holloway, *J. Phys. D: Appl. Phys.* 2008, **41**, 182002-1;
- 4 X. G. Peng, M. C. Schlamp, A. V. Kadavanich, A. P. Alivisatos, *J. Am. Chem. Soc.*, 1997, **119**, 7019;
- 5 L. Manna, E. C. Scher, L. S. Li, A. P. Alivisatos, *J. Am. Chem. Soc.* 2002, **124**, 7136;
- 6 X. Q. Meng, H. Peng, Y. Q. Gai, J. Li, *J. Phys. Chem. C* 2010, **114**(3), 1467;
- 7 D. Bera, P. H. Holloway, H. Yang, *ECS Trans* 2006, **3**(5), 5;
- 8 H. Yang, P. H. Holloway, *Appl. Phys. Lett.* 2003, **82**, 1965;
- 9 D. Bera, L. Qian, P. H. Holloway, *J. Phys. D: Appl. Phys.* 2008, **41**, 182002-1;
- 10 B. Sikora, K. Fronc, I. Kaminska, A. Baranowska-Korczyc, K. Sobczak, P. Dłużewski, D. Elbaum *J. Sol-Gel Sci. Technol.* 2012, **61**, 497;
- 11 Y. F. Li, B. Yao, Y. M. Lu, B. H. Li, Y. Q. Gai, C. X. Cong, Z. Z. Zhang, D. X. Zhao, J. Y. Zhang, D. Z. Shen, X. W. Fan, *Appl. Phys. Lett.*, 2008, **92**, 192116-1;
- 12 S. Rakshit, S. Vasudevan, *ACS Nano*, 2008, **2**(7), 1473-1479;
- 13 B. Valeur, *Molecular Fluorescence. Principles and Applications* **Ch. 9** Wiley-VCH, Weinheim (2002).
- 14 A. R. Clapp, I. L. Medintz, H. T. Uyeda, B. R. Fisher, E. R. Goldman, M. G. Bawendi, H. Mattoussi, *J. Am. Chem. Soc.* 2005, **127**, 18212;